ORIGINAL PAPER

Ammonium adsorption on Brønsted acidic centers on low-index vanadium pentoxide surfaces

Maciej Szaleniec · Agnieszka Drzewiecka-Matuszek ·
Małgorzata Witko · Paweł Hejduk

Abstract Vanadium-based catalysts are used in many technological processes, among which the removal of nitrogen oxides (NO_x) from waste gases is one of the most important. The chemical reaction responsible for this selective catalytic reaction (SCR) is based on the reduction of NO_x molecules to N_2, and a possible reductant in this case is pre-adsorbed NH_3. In this paper, NH_3 adsorption on Brønsted OH acid centers on low-index surfaces of V_2O_5 (010, 100, 001) is studied using a theoretical DFT method with a gradient-corrected functional (RPBE) in the embedded cluster approximation model. The results of the calculations show that ammonia molecules are spontaneously stabilized on all low-index surfaces of the investigated catalyst, with adsorption energies ranging from −0.34 to −2 eV. Two different mechanisms of ammonia adsorption occur: the predominant mechanism involves the transfer of a proton from a surface OH group and the stabilization of ammonia as an NH_4^+ cation bonded to surface O atom(s), while an alternative mechanism involves the hydrogen bonding of NH_3 to a surface OH moiety. The latter binding mode is present only in cases of stabilization over a doubly coordinated O(2) center at a (100) surface. The results of the calculations indicate that a nondirectional local electrostatic interaction with ammonia approaching a surface predetermines the mode of stabilization, whereas hydrogen-bonding interactions are the main force stabilizing the adsorbed ammonia. Utilizing the geometric features of the hydrogen bonds, the overall strength of these interactions was quantified and qualitatively correlated ($R = 0.93$) with the magnitude of the stabilization effect (i.e., the adsorption energy).

Introduction

V_2O_5-based catalysts are of great importance in the catalytic reactions used to care for and protect the environment, such as de-NO_x processes. These reactions are mainly responsible for the removal of the waste gases that are the products of liquid or gaseous fuel combustion [1]. The interest in using vanadium-based catalysts in industry is also a result of their resistance to SO_2 poisoning. One useful process is the selective catalytic reduction (SCR) of nitrogen oxides (NO_x) in the presence of ammonia, which can proceed either in the absence or in the presence of oxygen. Both processes are called "standard SCR" [2–20] and proceed according to the following equations:

$$6\ NO\ +\ 4NH_3 \rightarrow 5N_2 +\ 6H_2O$$
$$4NO + 4NH_3 + O_2 \rightarrow 4N_2 + 6H_2O.$$
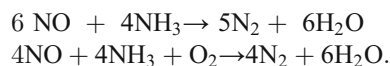
In 2002, the reaction mechanism of so-called fast SCR was proposed by Koebel et al. [21, 22] and by Madia et al.: [23]:

$$2NO + 2NO_2 + 4NH_3 = 4N_2 + 6H_2O.$$

In the fast SCR process, the catalyst is re-oxidized by nitrogen dioxide instead of by the oxygen molecule, and the rate of this reaction is ten times higher than that for the standard SCR process. However, such acceleration occurs only for the equimolecular NO and NO_2 mixture, and the reaction rate decreases dramatically if the fraction of NO_2 is

M. Szaleniec (✉) · A. Drzewiecka-Matuszek · M. Witko ·
P. Hejduk
Jerzy Haber Institute of Catalysis and Surface Chemistry, Polish
Academy of Sciences, Niezapominajek 8, 30-239 Kraków, Poland
e-mail: ncszalen@cyf-kr.edu.pl

larger than 50 %. In all SCR processes, side reactions such as NH_3 oxidation to NO, NO_2, or N_2O (competition with SCR at high temperature) or the formation of ammonium nitrate (catalyst poisoning) occur.

The mechanism of the standard SCR reaction, in which nitrogen oxide is reduced to pure nitrogen and water, is still not fully clear; therefore, this mechanism has been investigated extensively by both experimentalists and theoreticians. Many attempts to understand this process have been made in the last few years, and two mechanisms are postulated, namely the Eley–Rideal and Langmuir–Hinshelwood mechanisms. According to the Eley–Rideal mechanism [24–42], ammonia is adsorbed and activated at Brønsted centers. Next, an NH_3 species reacts with the gas-phase or weakly adsorbed NO molecule to yield a dinitrogen molecule and water, whereas the reduced surface (i.e., V–OH groups) is re-oxidized to V=O by O_2 from the gas phase or O from the bulk. The Langmuir–Hinshelwood mechanism [43–46] also postulates ammonia adsorption. However, NO is first oxidized by gaseous O_2 to NO_2, and then the reaction between the adsorbed ammonia and the adsorbed NO_2 species occurs. The reduced Brønsted centers are regenerated by a water molecule. Although these two mechanisms agree with the results of an experiment suggested by Topsøe et al. [2, 5], the SCR reaction proceeds according to both the Eley–Rideal and the Langmuir–Hinshelwood mechanisms. This conclusion is supported by the fact that NO molecules can be adsorbed at the coordinatively unsaturated metallic centers at the catalyst surface, thus reacting easily as weakly adsorbed species.

The main discussion in the literature concerns the forms of both the NH_3 and NO molecules. Table 1 lists the postulated

active forms of both substrates in the SCR reaction for different catalysts. In the case of the reactions catalyzed by pure V_2O_5, the NH_3 molecule is adsorbed at the Brønsted acid centers in the form of NH_4^+ cations, whereas NO is in the gaseous phase; the reaction occurs via the Eley–Rideal mechanism. However, the detailed mechanism of the simple activation of the ammonia molecule is still a matter of controversy, especially regarding the localization of the active sites responsible for this elementary step. Miyamoto and Inomata et al. [24–27] suggested that the active Brønsted centers are localized at the (010) surface of V_2O_5, whereas Gasior and Haber [42] indicated planes that host the surface OH groups. The existence of Brønsted acid sites at the unsaturated (001) and (100) faces of the V_2O_5 crystals was also confirmed by Andersson [51], who postulated that these net planes are responsible for the adsorption and dissociation of a water molecule, which consequently leads to surface hydroxylation. Moreover, Ozkan et al. [39–41] also demonstrated that the hypocoordinated (001) and (100) net planes of V_2O_5 serve as active faces in the SCR mechanism, and the (010) face is mainly responsible for the ammonia oxidation reactions. It has also been suggested that ammonia can be coordinatively adsorbed on the surface vanadium cations, which act as the Lewis acidic centers in the form of V–NH_3 or V–NH_2 species.

In this study, the first step in the selective catalytic reduction of NO_x by ammonia is discussed, mainly involving NH_3 adsorption on the surface OH groups (Brønsted acid centers) that are present at three low-index V_2O_5 surfaces. There have been a number of theoretical studies of the ammonia adsorption on Brønsted acid sites using both cluster [26, 49, 50, 52–58] and periodic [59, 60] approaches at different levels of theory, including the semiempirical level [26], post-Hartree methods [61], and the density functional theory level [49, 50, 52, 53, 55–61]. The conclusions from these investigations are similar and indicate that, in almost all cases, ammonia is stabilized at surface OH groups in the form of NH_4^+ cations, as postulated on the basis of experimental results. However, the above studies are focused only on the (010) V_2O_5 net plane, but it is known that vanadium crystals can expose other low-index surfaces, such as coordinatively unsaturated (100) and (001) surfaces. The fact that approximately 15 % of the overall contribution to the crystallite structure comes from these surfaces [62] indicates that unsaturated surfaces might play an important role in the catalytic process, as was postulated by Haber [42] and Ozkan [39–41]. The present paper discusses ammonia adsorption on OH centers of all three low-index V_2O_5 surfaces. Two different modes of ammonia stabilization are reported: (i) an NH_4^+ moiety hydrogen bonded to surface oxygen atoms and (ii) an NH_3 moiety hydrogen bonded to the surface OH group. The mode and strength of the ammonia stabilization over various adsorption sites are discussed in terms of the local electrostatic potential of the surface binding sites and the strength of the hydrogen bonds

Table 1 Forms of the activated NH_3 and NO species postulated to be involved in the SCR mechanism as a function of the catalyst used. Additionally, the table includes a list of postulated active centers thought to be responsible for the stabilization of ammonia

Active form of:		Catalyst	Postulated active center(s)	Reference(s)
NH_3	NO			
NH_4^+	NO_2 (ads)	V_2O_5	–	[43–45]
NH_4^+	NO (gas)	V_2O_5	V=O, V–OH	[24–27]
NH_4^+	NO (gas)	V_2O_5	V–OH, V–O–V	[42]
NH_4^+	NO (gas/ads)	V_2O_5/TiO_2	V=O, V–OH	[4, 47]
NH_3 NH_4^+	NO (gas)	V_2O_5	V=O, V=O V=O, V–OH V–OH, V–OH	[39–41]
V–O–NH_2	NO (gas)	V_2O_5/support	V=O, V=O	[35, 36]
V–NH_2	NO (gas)	V_2O_5/TiO_2	V=O	[48]
NH_3(ads) NH_2	N_2O (ads) NO (ads)	V_2O_5/support V_2O_5/TiO_2	Lewis acid centers	[46]
NH_4^+	NO (ads)	V_2O_5	V=O	[49]
NH_4^+	NO (ads)	$V_2O_5/WO4$	V=O/W=O	[50]

formed between the ammonia molecule and the surface oxygen atoms.

Models and computational details

Model setup

The crystal lattice of vanadium pentoxide has an orthorhombic symmetry and is assigned to the space group D_{2h}-P_{mmn}, with unit cell parameters defined as a=11.51 Å, b=4.37 Å, c=3.56 Å [63, 64]. The building unit forms a distorted octahedron with V–O bond distances varying between very short (1.58 Å, vanadyl groups) and very long (2.79 Å, van der Waals type bonding). Three possible low-index surfaces exist: the saturated (010) and unsaturated (001 and 100) surfaces are shown in Fig. 1.

The most thermodynamically stable (010) surface [62] (Fig. 1a) is characterized by three structurally different oxygen sites: (i) terminal vanadyl oxygen atoms O(1), which are singly coordinated to vanadium atoms and protrude from the surface in rows, and two bridging oxygen sites that are (ii) doubly, i.e., O(2), or (iii) triply, i.e., O(3), coordinated to vanadium centers. The unsaturated (001) surface (Fig. 1b), which is described by the existence of "valley"- and "hill"-like regions, exhibits coordinatively unsaturated vanadium atoms and three structurally different oxygen sites that lie in the plane (Fig. 1b): vanadyl oxygen O(1) and bridging O(2) or O^e(2) oxygen atoms coordinated to two vanadium atoms (the O^e(2) atom is connected to two vanadium atoms from different atomic layers and positioned on the surface edges). The unsaturated (100) surface may have a different termination [62]; the most thermodynamically stable structure is shown in Fig. 1c and contains unsaturated V centers and in-plane singly (O(1)) and doubly O(2)) coordinated sites.

The $V_{10}O_{31}H_{12}$ cluster (Fig. 2) was selected as a model of the (010) surface, as described in our previous studies [65], in order to discuss electronic/adsorption properties of the (010) net plane. To mimic the (001) V_2O_5 surface, the $V_{21}O_{65}H_{25}$ cluster was used to describe both the "hill" and "valley" regions (Fig. 2). The $V_{16}O_{52}H_{24}$ cluster (Fig. 2) was chosen as the most appropriate model to characterize the (100) V_2O_5 net plane [65]. For all clusters, the dangling bonds of the peripheral O atoms were saturated with H atoms, forming OH groups and neutralizing the clusters [66, 67]. All initial clusters selected as surface models were closed shell. To prepare sites for ammonia adsorption, an additional H atom was added to the selected surface oxygen sites, thus forming surface OH groups and leading to the doublet systems [56, 68]. This procedure simulated the mechanism of surface OH formation under the reaction conditions (e.g., by dissociative adsorption of H_2O [69] or the reaction of NH_3 and NO on the V^{5+}=O sites [70]).

Calculation procedure

The program StoBe, the local version of DeMon, was applied to perform the calculations [71]. This used an ab initio density functional theory (DFT) method in which the Kohn–Sham orbitals were represented by a linear combination of atomic orbitals (LCAOs). For constrained geometry optimization of all cluster models, we applied the revised version of the gradient corrected functional of Perdew–Burke–Ernzerhof (RPBE) [72, 73] with all-electron DZVP basis sets of contracted Gaussians [74, 75]. This functional proved suitable for studying the interactions of small molecules with a broad range of adsorption sites, ranging from metal oxides to transition metal complexes [69, 76–81]. Models were subjected to partial geometry optimization using the Broyden–Fletcher–Goldfarb–Shanno (BFGS) algorithm according to the procedure described in [65]. In short, only the local environment near to each oxygen adsorption site was allowed to relax for both H and NH_3 absorption. The local environment of a particular oxygen was defined by its nearest V neighbors together with the oxygen atoms linked to these metal atoms and the adsorbate molecule. The rest of the atoms were kept frozen at their crystallographic positions. The vibration analysis for the final V_2O_5–H–NH_3 complexes was performed only for the geometry-relaxed sections, and no imaginary frequencies indicating local energy minima were observed.
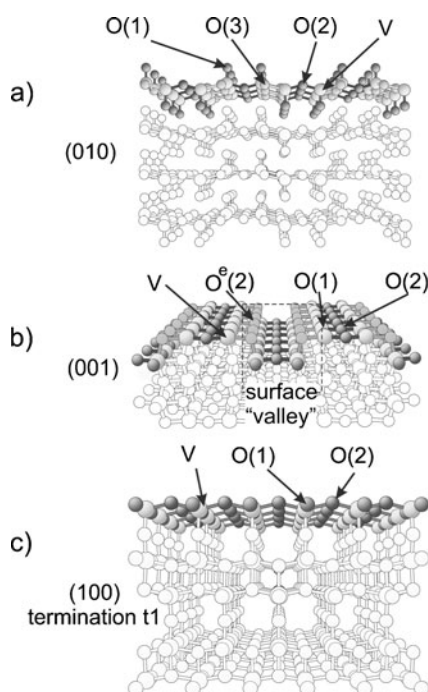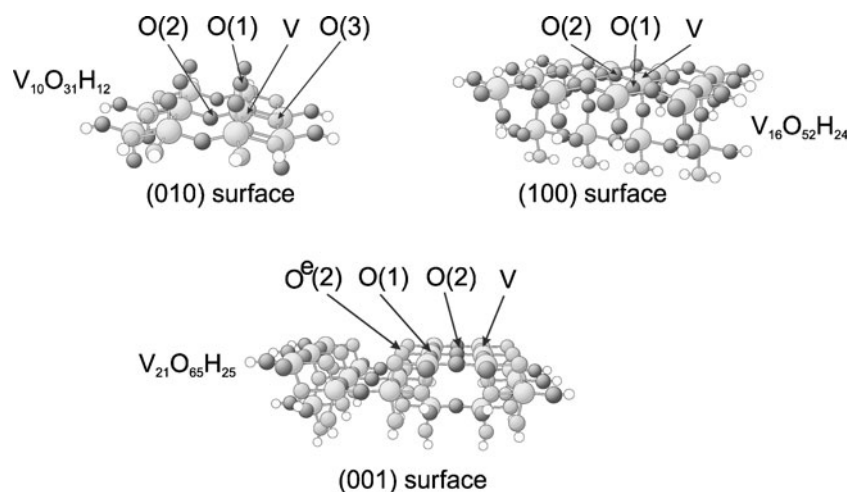

Fig. 1a–c Three possible low-index surfaces: **a** saturated (010) and **b** unsaturated (001) and (100). The annotation describes the type of atoms involved, with their coordination number shown in parentheses. The superscript ^{e} indicates "edge" localization of the O^e(2) oxygen atom

Fig. 2 Structural models of the clusters used in this study

(010) surface

(100) surface

(001) surface

The structure of the model with an OH group was obtained by adding the hydrogen atom to a particular oxygen site and then performing geometry relaxation, as described in [82]. Hydrogen becomes stabilized at all oxygen sites present on three low-index V_2O_5 surfaces, with this process being spontaneous, as shown by periodic calculations [83]. The figures presenting the structures of clusters with adsorbed hydrogen atoms are provided in the "Electronic supplementary material" (ESM; Figs. S1–S3).

A detailed analysis of the electronic structure of each cluster was performed using the charge density distribution (Mulliken populations) [84], the Mayer bond orders [85, 86], and an analysis of electrostatic potentials. The electrostatic potentials were calculated 2 Å above each adsorbed hydrogen atom (i.e., x,y coordinates of the hydrogen atom). Such an approach provided a uniform and objective method for estimating the electrostatic interaction of the local surface with an NH_3 molecule before a hydrogen bond is formed, which can result in the potential transfer of the H^+ from the surface OH to the adsorbate. On the other hand, in order to estimate the electrostatic interaction of the surface with the already adsorbed NH_4^+/NH_3 moiety, the electrostatic potential was calculated for the respective surface (i.e., "bare" or with an OH group) at the coordinates of the N atom of the adsorbate.

The ammonia adsorption energies were calculated according to the following equation:

$$E_{ads} = E_{tot}(cluster + NH_3) - [E_{tot}(cluster) - E_{tot}(NH_3)], \quad (1)$$

where $E_{tot}(cluster)$ denotes a cluster with a Brønsted acid OH group.

These adsorption energies were corrected for London dispersion forces that are not included in RPBE with the DFT+D2 procedure using empirical damped dispersion correction [87].

A global scaling factor of 1.25 (s6) was used for RPBE calculations and 0.75 for geometries optimized with the PBE functional [81, 88].

Model validation

The influence of the basis set on the adsorption energies calculated with the RPBE functional was investigated by performing RPBE/TZVP single point calculations for the (010) net plane.

In order to cross-validate the performance of the RPBE functional, we conducted test calculations for NH_3 adsorption on O sites of the (010) net plane in Turbomole v.6.3 [89] with the gradient-corrected Perdew–Burke–Ernzerhof (PBE) functional [90–93] and the def-TZVP all-electron basis set [94]. The resolution of identity (RI) approach was applied to compute the electronic Coulomb interactions [95, 96]. Complete geometry optimization was performed for the (010) models with the exception of terminal oxygen atoms terminated with hydrogen atoms. The positions of terminal O and H atoms were frozen in order to preserve the structural constraints imposed by the surface structure. The locations of energetic minima were confirmed by vibration analysis and by checking for a lack of imaginary frequencies. The structures of the respective models with adsorbed hydrogen and ammonium ion are presented in the ESM (Figs. S4 and S6).

Similar optimizations of unsaturated (001) and (100) model surfaces were not possible, as they led to significant surface reconstruction and yielded an artificial geometry for the V_2O_5 surface. Comparison of the obtained reconstructed surface structures with model net planes obtained with periodic calculations [83, 97] showed that the partially constrained cluster models described the surface more accurately than the relaxed models in which boundary constraints were imposed. The reconstructed geometries obtained for the (001) and (100) net planes are provided in the ESM.

Results and discussion

The ammonia is stabilized via O–H–N hydrogen bonds with surface hydroxyl groups present at each low-index V_2O_5 surface. However, the adsorption mechanism and adsorption geometry depend on both the type of center and the type of net plane involved (see Tables 2, S2, and 5).

Table 2 summarizes the data obtained for the process of ammonia adsorption at the three discussed low-index V_2O_5 surfaces. It contains the adsorption energies ($E^{ads}(NH_3)$) and Mulliken atomic charges (Q), while Table S2 in the ESM contains the Mayer bond orders (BO) and the distances (R) and angles (α) of the N···H···O hydrogen bonds.

NH_3 adsorption at a (010) V_2O_5 surface

At the (010) V_2O_5 surface, ammonia is adsorbed as an NH_4^+ cation and stabilized by single or double hydrogen bonds (see Fig. 3 and Figure S4 of the ESM). In all of the studied cases, ammonia is spontaneously adsorbed at each of the adsorption sites (Table 2). The adsorption energies $E^{ads}(NH_3)$ attain negative values: −0.98 eV, −1.07 eV, and −1.31 eV (−30.2, −22.6, and −24.7 kcal/mol^{-1}, respectively) for stabilization at the O(2), O(3)–O(2), and O(1)–O(1) centers, respectively. The largest adsorption energy (−1.31 eV) is observed for the stabilization of two O(1) oxygen sites. The introduction of the correction for London dispersion forces does not change the qualitative results, i.e., the largest adsorption energy is observed for two O(1) oxygen sites (−1.44 eV) followed by O(3)–O(2) (−1.39 eV) and O(2) (−1.40 eV). Moreover, the calculation of adsorption energies at the RPBE/TZVP level also does not change the qualitative description of the adsorption, yielding −0.66 eV, −0.88 eV, and −1.02 eV eV at the O(2), O(3)–O(2), and O(1)–O(1) centers, respectively.

When NH_3 approaches the V-O(1)H Brønsted acidic group it becomes tilted and is stabilized in the bi-dentate form by two hydrogen bonds with hydrogen donor-acceptor distances (O(1)–N) of 2.55 Å and 2.78 Å and N–H–O angles equal to 170° and 155°, respectively (Fig. 3). The proton of the surface O–H group is shifted toward NH_3 (the O–H distance is

elongated from 0.98 to 1.55 Å, and the BO is weakened from 1 to 0.18) and an H bond is formed with NH_4^+ acting as a donor and the surface O atom as the H-bond acceptor. A second hydrogen bond is formed between a hydrogen atom of ammonia and the other vanadyl O(1) oxygen atom (d(H—O)=1.7 Å, BO=0.15).

A similar type of bidentate stabilization is observed when ammonia approaches an O(3) site. The hydrogen-bonding interactions with O(3)–H and O(2)–H lead to the formation of two bonds (Fig. 3) with O···N distances of 2.63 and 2.84 Å and NHO angles equal to 165° and 133°, respectively. The O–H and N–H bond distances/bond orders are 1.55/0.15 and 1.10/0.71 for the first hydrogen bond and 2.03/0.06 and 1.04/0.87 for the second hydrogen bond, again indicating the transfer of the proton from the O(3)–H group to the ammonia and its stabilization in the cationic form. Finally, for the adsorption site above the surface O(2)H group, only one single hydrogen bond is created, with an O···N distance of 2.60 Å and an NHO angle of 175°. The O–H and N–H bond distances/bond orders are 1.48/0.18 and 1.12/0.66, which suggests the formation of an NH_4^+ species.

The formation of ammonium cations (NH_4^+) is further supported by the results of a Mulliken population analysis (see Table 2). The charge on the NH_4^+ species when it is stabilized at an O(1)–O(1), O(2), or O(3)–O(2) site is +0.81, +0.87, or +0.87, respectively. This result demonstrates that, in each case, the proton is abstracted from the surface OH group and shifted toward the nitrogen atom. As a result, NH_4^+ groups are formed and act as proton donors in the newly created $H_3N–H\rightarrow O$ hydrogen bonds.

The introduction of corrections for dispersion forces lowers the adsorption energy of each site by 0.13–0.34 eV (3.1–7.8 kcal/mol^{-1}). The dispersion attraction appears to be higher for an ammonia ion adsorbed in between double rows of V=O ligands (around 0.3 eV), i.e., for O(2) and O(3), O(2) sites, than for an ammonia ion adsorbed on two O(1) oxygen atoms (0.13 eV). As a result, all three adsorption sites exhibit similar ammonia adsorption energies of 1.32–1.44 eV, although the overall preference for the O(1) site is still maintained. These calculations indicate that, in the case of ammonia ions adsorbed

Table 2 DFT (RPBE/DZVP) and DFT+D2 corrected energies of ammonia adsorption and NH_3/NH_4^+ charges. The Mulliken charge on the adsorbed ammonia was calculated both with and without the H atom from the OH group as $Q(NH_4)$ and $Q(NH_3)$, respectively

	(010) surface			(100) surface		(001) surface	
Adsorption site	O(1), O(1)	O(2)	O(3), O(2)	O(1)	O(2), O(2)	O(2)	Valley O^e(2), O^e(2), O^e(2)–O(1)–O(1)
E_{ads} DZVP (eV)	−1.31	−0.98	−1.07	−0.86	−0.70	−0.49	−1.97
E^{ads}+D2^{corr} (eV)	−1.44	−1.32	−1.40	−1.07	−1.03	−0.72	−2.29
Mulliken population:							
$Q(NH_3)$	+0.48	+0.45	+0.47	+0.41	+0.48	+0.14	+0.60
$Q(NH_4)$	+0.81	+0.87	+0.87	+0.82	+0.83	+0.58	+0.87

Fig. 3 Geometries of ammonia adsorption on the (010) V_2O_5 model surface. The NH_4^+ cations are stabilized by either a single hydrogen bond with an O(2) atom or double hydrogen bonds with O(3) and O(2) or two O(1) oxygen atoms. The geometries obtained for $V_{10}O_{31}H_{12}$ are translated to the model (010) surface for visualization purposes. The adsorption geometries on the $V_{10}O_{31}H_{12}$ are presented in Fig. S1 of the ESM
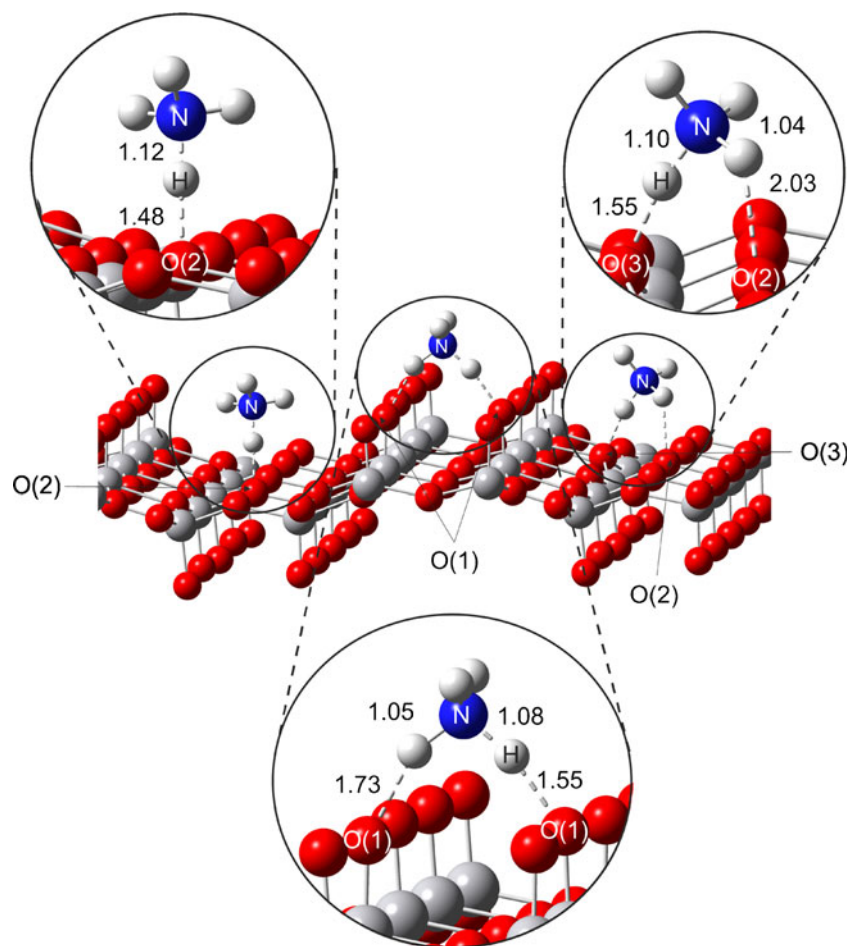
on O(2) and (O3) sites, dispersion accounts for ~25 % of the stabilization, while dispersion accounts only for 10 % of the stabilization of ions adsorbed on the tops of O(1) rows.

The above results demonstrate that, at the (010) surface, ammonia is activated according to the same mechanism at Brønsted acid centers. NH_4^+ cations act as proton-donating groups in the hydrogen bonds. The formation of hydrogen bonds plays a vital role in ammonia stabilization. Our results are consistent with the recent DFT calculations of Sun et al. [50] and Yuan et al. [49], which showed energetically favorable stabilization of NH_4^+ cations by two hydrogen-bonding interactions with O(1) atoms. However, because the clusters used in those studies were very small ($V_2O_9H_8$ and $V_6O_{20}H_{11}$, respectively), the authors could not study adsorption at the O(2) or O(3) sites.

NH_3 adsorption at the (100) V_2O_5 surface

At the (100) surface, NH_3 is stabilized at the surface hydroxyl groups O(1)H and O(2)H (Fig. 4). In analogy to the (010) V_2O_5 surface, ammonia undergoes spontaneous adsorption with $E^{ads}(NH_3)$ values of −0.86 and −0.70 eV (−19.8 and

−16.1 kcal/mol^{-1}) for stabilization at the O(1) and O(2) centers, respectively, while the dispersion-corrected adsorption energies are −1.07 and −1.03 eV (−24.6 and −23.8 kcal/mol^{-1}) for stabilization at the O(1) and O(2) centers, respectively.

Adsorption at Brønsted acidic vanadyl sites (V–O(1)H) leads to the creation of a single hydrogen bond with a hydrogen donor–acceptor distance (O(1)···N) of 2.54 Å and an NHO bond angle of 179°. At the second adsorption center localized above the surface O(2)H site, ammonia is stabilized by two hydrogen bonds formed between two bridging O(2) oxygen atoms. One strong hydrogen bond is formed between O(2) and an ammonium cation with an O(2)···N distance of 2.67 Å and an NHO angle of 175°, and the other—weaker—hydrogen bond is formed with O(2) from a parallel atomic row and has an O(2)···N distance of 2.95 Å and an NHO angle of 178°.

The mechanism of stabilization is similar for both sites, namely the protons shift from the O sites to the ammonia molecule and the formation of NH_4^+ is observed.

The cationic form is substantiated by the Mulliken population and a geometry analysis. The total charge on the NH_4^+ species is +0.82 for O(1) and +0.83 for the O(2) site.

Fig. 4 Geometries of the ammonia adsorption sites on the (100) V_2O_5 model surface. The NH_4^+ cations are stabilized by a single hydrogen bond with O(1) and by two hydrogen bonds with two O(2) oxygen atoms. The geometries were obtained for the $V_{16}O_{52}H_{24}$ cluster, and the position of the NH_4^+ at O(1) was moved to the edge of the cluster for visualization purposes
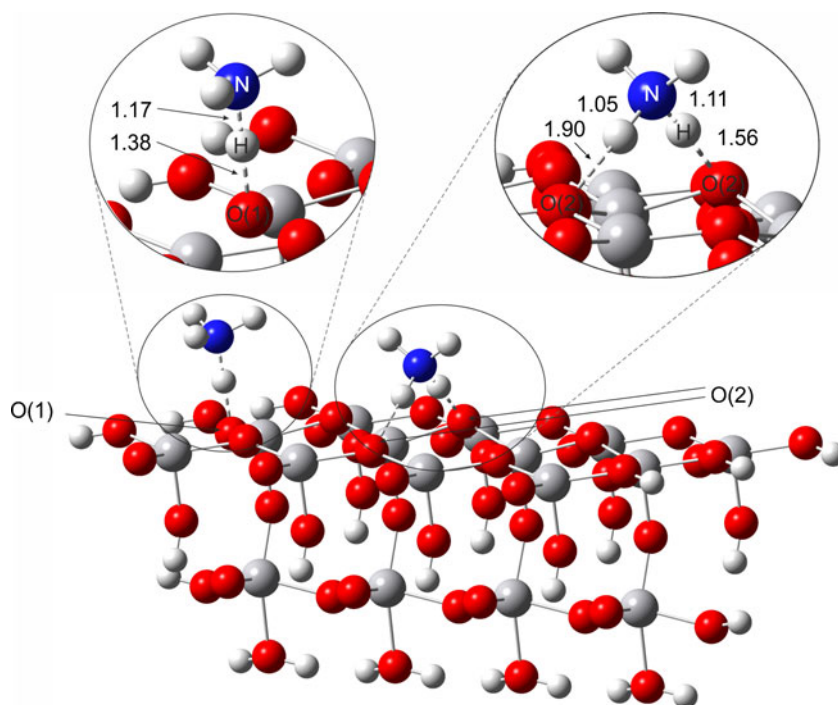
In the hydrogen bond formed at O(1), the N–H distance is fairly long (d(N–H)=1.17 Å, BO=0.56), whereas the interaction between the hydrogen and oxygen occurs at a short distance and is strongly covalent (d(H–O) 1.38 Å, BO=0.29).

In the case of the O(2) site, the stronger hydrogen bond is characterized by an N–H distance of 1.11 Å (BO=0.70) and an H–O distance of 1.56 Å (BO=0.20). The weaker hydrogen bond has a shorter N–H distance (1.05 Å, BO=0.82) and a longer H–O distance (d(H–O) 1.90 Å, BO=0.08). The stronger H-bonding at O(2) results in closer contact of the ammonium ion with the V_2O_5 surface than in the case of the O(1) binding site. As a result, the dispersion forces contribute more to stabilizing the adsorption, lowering the overall energy by −0.33 eV (−7.7 kcal/mol[-1]) for the O(2) binding site, as compared to −0.21 eV (−4.8 kcal/mol[-1]) for the O(1) site.

NH_3 adsorption at the (001) V_2O_5 surface

At unsaturated (001) V_2O_5 surfaces, the net plane process of ammonia adsorption is more complex because NH_3 is stabilized by single and triple hydrogen-bonding interactions that also be trifurcated toward different donors. As was the case for the two other low-index faces of V_2O_5, the E^{ads}(NH_3) energies indicate that the adsorption of ammonia on Brønsted acid centers at the (001) surface is spontaneous. The adsorption energies E^{ads}(NH_3) (Table 2) are −0.49 eV (−11.3 kcal/mol[-1]) and −1.97 eV (−45.4 kcal/mol[-1]) for the ammonia stabilization at the "hill"-like O(2) and the valley-like O^e(2), O^e(2),O^e(2)–O(1)–O(1) oxygen sites. The dispersion correction lowers the adsorption energy by −0.21 and

−0.31 eV (−5.2 and −7.3 kcal/mol[-1]) for the hill and the valley regions, respectively. The London attraction force for the hill-like O(2) site is comparable with the dispersion stabilization observed for the (100) O(1) site and twice as big as that calculated for O(1),O(1) sites on the (010) net plane. Interestingly, for valley-like adsorption sites, where ammonia ions seem to have the highest degree of van der Waals contact, the overall stabilization is only −0.32 eV, which is in the range of dispersion stabilization observed for O(2) sites on the (010) or O(2),O(2) sites on the (100) net plane.

Tables 2 and 5 list the stabilization energies and characteristics of the hydrogen bonds, and the geometries of the adsorbed NH_3 molecules are plotted in Fig. 5. Two different mechanisms of stabilization are observed on this surface: H_3N–H→O and O–H→NH_3. The former mechanism occurs for the adsorption sites localized above the surface valley-like region. These adsorption minima are populated independently of the starting geometries, i.e. when NH_3 approaches O(1)H or O(2)^{e}H, there is a proton shift from the surface OH groups to the ammonia molecule. After formation, the NH_4^+ cation migrates from the former OH site toward the valley region, where it is stabilized by multiple hydrogen-bonding interactions and favorable attractive electrostatic interactions (vide infra).

The ammonium ion (charge +0.87) forms two single hydrogen bonds with the O(2)^e atoms from two opposite hill regions with N···O distances of 2.70 Å and 2.72 Å and NHO angles of 173.2° and 174.3°. In addition, a weak trifurcated hydrogen-bonding interaction with one O(2)^e atom and two O(1) atoms from the bottom of the valley occurs. The N···O

Fig. 5 Geometries of the ammonia adsorption sites of the (001) V_2O_5 model surface. The NH_4^+ cation is stabilized by multiple hydrogen bonds involving three $O^e(2)$ and two O(1) atoms, whereas the NH_3 molecule is stabilized by a single hydrogen bond with an O(2) oxygen atom. The geometries were obtained from the $V_{21}O_{65}H_{24}$ cluster
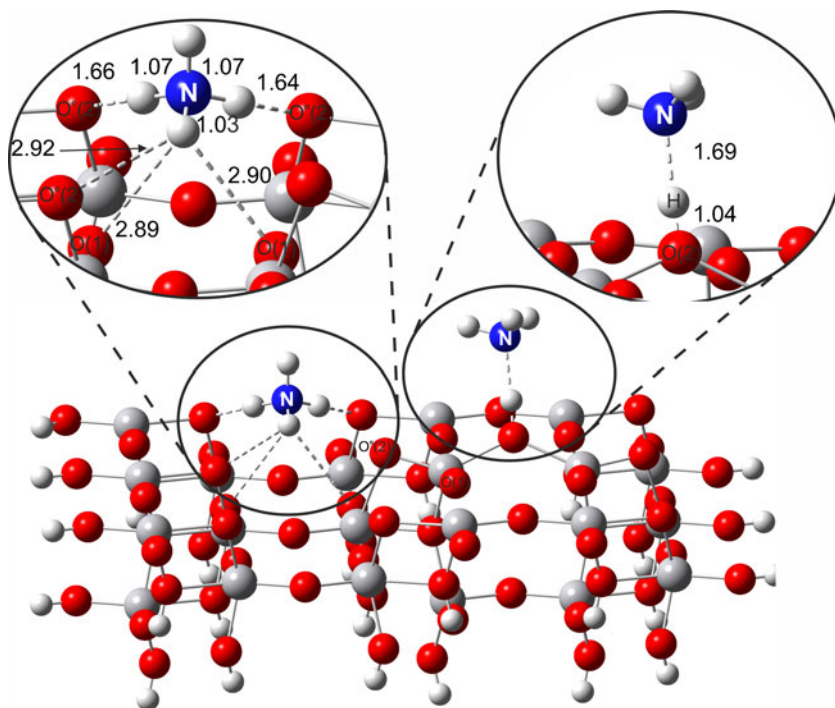
distances are 3.72 Å, 3.34 Å, and 3.30 Å and the NHO angles are 135.5°, 106°, and 105°, respectively. Moreover, the Mayer bond indices suggest that the N–H bonds (0.76–0.89) have higher covalences than the H–O bonds (0.1 for strong bonds, 0.01 for weak trifurcated bonds) do. Finally, small contributions to the adsorption energies also seem to be introduced by the interactions of NH_4^+ with surrounding V atoms. Although each of these interactions is characterized by a very small Mayer index (in the range of 0.007–0.016), the overall sum of the bond orders calculated for all three H atoms pointing into the valley equals 0.13, a value which is comparable with the strength of one hydrogen bond.

The latter O–H→NH_3 mechanism is present only for the stable position localized in the "mountain"-like region of the (001) net plane, i.e., over the surface O(2)H group. Such a mode leads to the formation of a monodentate hydrogen bond (d(N⋯O) 2.71 Å, NHO angle 165.8°). The surface O–H acts as a proton donor (d(O–H)=1.04 Å, BO=0.69), forming a long hydrogen bond of moderate strength (d(H–N)=1.69, BO=0.15). The NH_3 species remains almost neutral (+0.14), indicating an O–H→NH_3 mechanism of hydrogen-bond formation. An inspection of the adsorption geometry at the O(2) site suggests that, in this case, the hydroxyl group is a proton donor; the H atom remains closer to the surface O atom than to the nitrogen atom from the ammonia molecule.

NH_3 adsorption at the fully relaxed (010) V_2O_5 surface

The optimization of NH_3 adsorption at the PBE/TZVP level of theory yielded qualitatively the same results as those obtained

for RPBE/DZVP calculations, i.e., adsorption in the form of the NH_4^+ ion after proton transfer from the surface OH group to NH_3 (see Table 3 and Table S3 in the ESM). As in previous (010) models, the most energetically favorable adsorption site was localized over O(1), the next most favorable was over O(3), O(2), and the least favorable was over O(2) (−1.58, −1.02, and −0.89 eV, respectively). The introduction of dispersion corrections did not change that trend (−1.72, −1.25, −1.16 eV, respectively). Similarly to RPBE models, the smallest D2 correction was observed for NH_4^+ adsorbed over V=O(1) ligands due to its relatively long distance from the V_2O_5 surface.

However, the application of a different optimization algorithm implemented in Turbomole, as well as a more diffuse basis set, led to some minor changes in the geometry of the NH_4 ions that resulted in greater H-bond interaction (Fig. 6).

The tilt of the ammonia ion for the O(1),O(1) adsorption site becomes bigger than in RPBE model, which results in the presence of an additional bifurcated H-bond interaction of the third H atom with two O(1) atoms. This bifurcated bond is relatively weak, with H–O Mayer bond orders of 0.041 and 0.044 and H–O bond distances of 2.2 Å. Similarly, the ammonia is tilted over O(2) sites, which enables the formation of two weak H-bond contacts with O(3) oxygen atoms (BO = 0.036, d(H–O) = 2.33 Å). Finally, also in the case of NH_4^+ adsorption over O(3) sites, aside from two strong H-bonds with O(2) and O(3) oxygen atoms (H–O BO = 0.14 and 0.1, d(H–O)=1.74 and 1.78 Å, respectively), it was possible to detect the formation of one weak H-bond between a third hydrogen atom and an O(2) oxygen atom (BO=0.047, d(H–O)=2.1 Å).

Table 3 DFT (PBE/TZVP) and DFT+D2 corrected energies of ammonia adsorption over the (010) net plane and NH_3/NH_4^+ charges calculated without and with H atoms adsorbed on the surface

|	(010) surface		
Adsorption site	O(1),O(1) 2×O(1)	O(2), 2×O(3)	O(3),O(2), O(2)
E_{ads} (NH$_3$) (eV)	−1.58	−0.89	−1.02
E_{ads}(NH$_3$) (kcal/mol^{-1})	−36.4	−20.6	−23.5
E^{ads}+D2^{corr} (eV)	−1.72	−1.16	−1.25
E^{ads}+D2^{corr} (kcal/mol)	−39.8	−26.7	−28.8
Mulliken population:			
Q(NH$_3$)	+0.48	+0.49	+0.53
Q(NH$_4$)	+0.75	+0.79	+0.81

Summing up, the calculations performed with almost full optimization of cluster geometry and with the application of the TZVP basis set led to similar results to those seen for models with only local geometry optimization and in which the DZVP basis set was applied. It seems that the main reason for the observed geometry differences stem from the different geometry optimization algorithms implemented in the Stobe and Turbomole codes.

NH$_3$ binding mechanism

There has been a long ongoing discussion in the literature concerning a form of adsorbed ammonia (see Table 1) [18]. Our results indicate that at low-index V$_2$O$_5$ surfaces, two types of adsorption over Brønsted acid (surface OH) centers may occur: (i) ammonia as a positively charged NH$_4^+$ cation with a surface O site acting as a hydrogen acceptor, or (ii) ammonia as a neutral NH$_3$ molecule with a surface OH group acting as a hydrogen donor. Although hydrogen bonds are clearly the main force stabilizing the adsorbed ammonia, the local electrostatic characteristics of the surface where NH$_3$ contacts the OH group seem to determine the final form of the stabilized ammonia (i.e., either neutral or cationic).

Fig. 6 Geometries of ammonia adsorption on the (010) V$_2$O$_5$ model surface, calculated at the PBE/TZVP level of theory with full optimization of the surface. The NH$_4^+$ cations are either stabilized by hydrogen bonds with an O(2) atom and two O(3) atoms, hydrogen bonds with one O(3) and two O(2) atoms, or two strong H-bond interactions with O(1) oxygen atoms and one weak bifurcated H-bond with two O(1) atoms. The geometries obtained for V$_{10}$O$_{31}$H$_{12}$ are translated to the model (010) surface for visualization purposes. The adsorption geometries on the V$_{10}$O$_{31}$H$_{12}$ are presented in Fig. S2 of the ESM
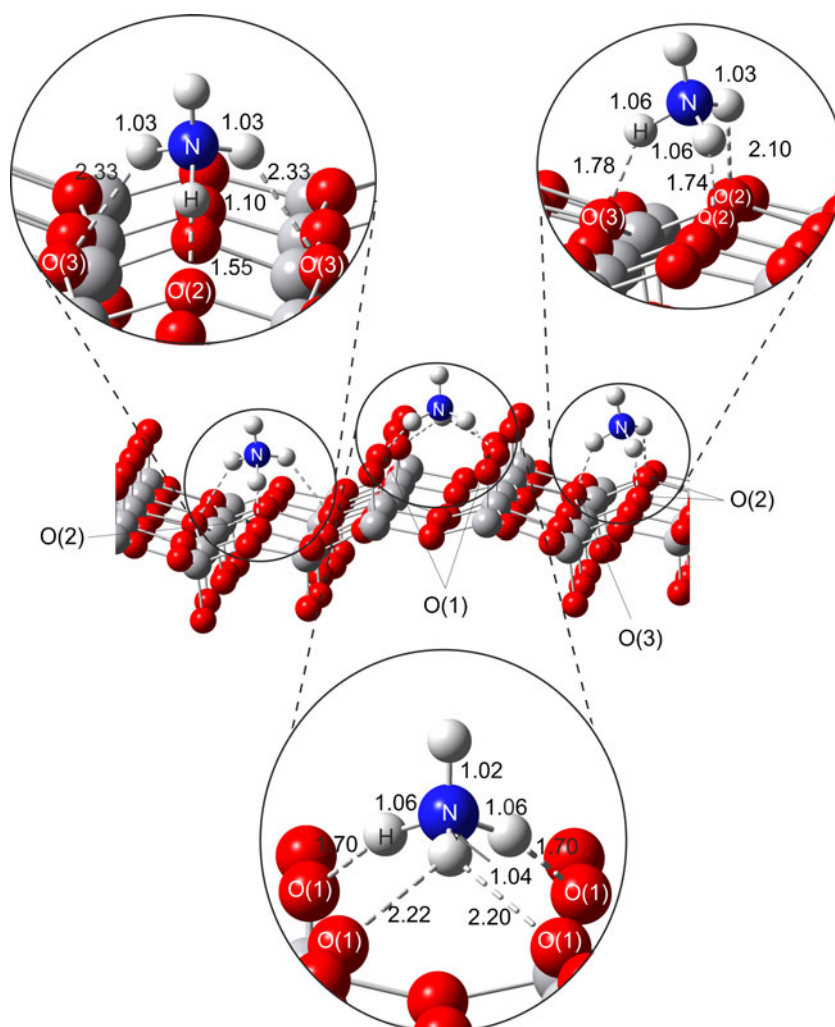
This effect is especially visible in the case of a (001) low-index surface, which has varied electrostatic characteristics (i.e., some regions of positive and negative electrostatic potential are present) [65]. If the neutral NH_3 approaches Brønsted sites, it can accept a proton from the OH group to attain a positive charge. As a result, a decrease in the electrostatic potential of the adsorption sites is observed due to the local accumulation of a negative charge at the deprotonated Brønsted site (Table 4). Naturally, the electrostatic interaction becomes significant between the positively charged ammonium cation (Mulliken charge ca. 0.8) and the local negatively charged surface. As a result, the adsorption energy decreases further due to the attractive electrostatic interaction of the positive charge of the ammonium cation with the negative electrostatic potential produced by the surface.

For surface sites with a very stable or strong positive electrostatic potential that is insensitive to the OH protonation state, such a proton shift would result in an increase of the system energy due to the repulsive electrostatic interaction (i.e., an interaction of a positively charged surface with an NH_4^+ cation). Therefore, in such cases, ammonia remains in an almost neutral form (i.e., an NH_3 molecule with a small charge of ca. +0.2, which results from NH_3 acting as a hydrogen-bond acceptor), minimizing the increase in the total energy due to the unfavorable, repulsive electrostatic interactions. Similar conclusions have been drawn by Calatayud et al. [98], who have used electrostatic potential as a reactivity index for V_2O_5 gas-phase clusters as well as unsupported and TiO_2-supported (010) V_2O_5 surfaces. This approach allowed spatial mapping of the regions that are most susceptible to electrophilic attack and, in accordance with our results, pointed to the region between terminal (O1) oxygen atoms.

This observation can be studied in a more quantitative manner if one considers the change in the potential electrostatic energy upon shifting the proton from the OH site toward the approaching NH_3. Table 4 contains electrostatic potentials calculated at a distance of 2 Å above the hydrogen atom of each OH group for the studied surface. These potentials approximate the electrostatic environment affecting the NH_3 molecule approaching the surface (i.e., before the hydrogen bond is formed). The electrostatic potentials are determined for surfaces with an adsorbed hydrogen atom (V^{OH}) and a "bare" V_2O_5 surface (V^{bare}) without an adsorbed hydrogen atom. The change in potential energy ΔPE upon shifting the proton from the surface OH group to NH_3 is approximated as the difference between the electrostatic potential energy (PE) of NH_4^+ over a bare V_2O_5 surface and the PE of NH_3 over the OH group from the surface with an adsorbed hydrogen atom.

$$\Delta PE = PE\ NH_4^+ - PE\ NH_3 = V^{bare}q^{NH4+} - V^{OH}q^{NH3},$$

where q^{NH4+} represents the average charge on the adsorbed ammonium cations (+0.86) and q^{NH3} represents the charge on the adsorbed ammonia (+0.14) over the O(2) site at the (001) net plane. Thus, ΔPE describes the gain (or loss) in the electrostatic energy due to the transfer of a hydrogen from a surface OH group to an NH_3 molecule.

The transfer of a hydrogen in the form of a proton occurs when ΔPE is negative, ensuring strong electrostatic stabilization of the positively charged ammonium cation. In most of the cases studied, the change in electrostatic energy following the hydrogen shift is highly negative (from approximately −0.4 to −0.9 eV), which results in a thermodynamic preference for NH_4^+. However, for O(2) sites at a (001) surface, there is no energy gain connected with the hydrogen shift because the ΔPE attains a positive value (+0.03 eV). As a result, the ammonia is stabilized in its neutral form. Notably, at a (001) surface, the site of the proton shift is distant from the

Table 4 The electrostatic characteristics of ammonia adsorption over the Brønsted sites of the (010), (100), and (001) V_2O_5 model surfaces

Surface	(010)			(100)		(001)		
Adsorption site	O(1)	O(2)	O(3)	O(1)	O(2)	O(2)	O(1)	$O^e(2)$
Ads. species	NH_4^+	NH_4^+	NH_4^+	NH_4^+	NH_4^+	NH_3	NH_4^+	NH_4^+
Q	0.81	0.87	0.87	0.82	0.83	0.14		
V^{OH}	−0.14	0.63	0.59	−0.22	0.33	0.42	0.16	0.55
V^{bare}	−1.07	−0.68	−0.55	−0.84	−0.38	0.12	−0.47	−0.57
PE(NH_3)	−0.02	0.10	0.09	−0.04	0.05	0.07	0.03	0.09
PE(NH_4^+)	−0.92	−0.58	−0.47	−0.72	−0.33	0.10	−0.40	−0.49
ΔPE	−0.90	−0.68	−0.56	−0.68	−0.38	0.03	−0.43	−0.58

Ads. species (NH_4^+/NH_3): form of ammonia moiety; Q: overall charge on the ammonia moiety; V: electrostatic potential (eV) calculated for the position of the N atom of the adsorbed ammonia over the hydrogenated (OH) and nonhydrogenated (bare) V_2O_5 model surfaces; *PE*: potential electrostatic energy (eV) of the adsorbed ammonia (PE(NH_3)) or the ammonium ion (PE(NH_4^+)) over the hydrogenated and nonhydrogenated surfaces, respectively; *ΔPE*: difference between PE(NH_4^+) and PE(NH_3) in eV. The average charges used for the calculation of ΔPE are 0.86 for NH_4^+ and 0.16 for NH_3

final, most favorable adsorption site. Regardless of the initial starting place of the NH$_3$ molecule (i.e., over O(1) or O^e(2)), the proton is shifted from the surface OH group. To probe the electrostatic influence of the surface on the proton shift process, the electrostatic potentials were calculated at distance of 2 Å above the H atoms adsorbed at the O^e(2) and O(1) sites. The results are collected in Table 4.

As observed from Table 4, the positive potential of the surface with the adsorbed H atom becomes negative (changing from 0.16 eV to −0.47 eV for the O(1) site and from 0.55 eV to −0.57 eV for the O^e(2) site). This result explains why ammonia becomes an ammonium cation at those sites. However, the vicinity of the deep negative potential well at the center of the valley (−1.58 eV for the NH$_4^+$ absorption site) attracts the cations to the most energetically favorable position.

Thus, the surface electrostatics influence the form of the stabilized ammonia. The local surface electrostatics of the spot at which ammonia contacts the surface determines whether the proton transfer will occur. If the proton is shifted, the ammonium cation can migrate further across the surface to maximize the electrostatic and hydrogen-bond interaction energies, as exemplified by a model of the adsorption over the O(1) and O^e(2) over (001) surface.

Quantitative modeling of adsorption energies

As shown above, the stabilization of ammonia over the Brønsted acid sites originates from the hydrogen bonds and is sensitive to the surface electrostatics. An interesting question arises as to whether it is possible to predict the strength of each adsorption site (i.e., the adsorption energy) based on a knowledge of the hydrogen-bond strength (derived only from geometry parameters) and on the local electrostatic potential. Theoretically, such a model would allow for the estimation of the relative importance of the forces (i.e., hydrogen bonds versus electrostatic) involved in the stabilization of ammonia over the V$_2$O$_5$ surface. Moreover, such a model would allow estimation of the adsorption site strength based solely on the geometry of the final structure of the V$_2$O$_5$-OH–NH$_3$ complex without the need to calculate the geometry and energy of the V$_2$O$_5$–OH reference model (thus shortening the calculation procedure). The usefulness of the electrostatic potential for predicting adsorption phenomena (such as interaction energies) has already been demonstrated by Tielens and Geerlings [99].

To build such a semiquantitative structure–property relationship (QSPR) model, each hydrogen-bond strength was described according to the methodology of the hydrogen bond analysis proposed by Jeffrey [100, 101], who studied a large number of hydrogen bonds and demonstrated that the energy of the particular bond varies between 0.2 and 40 kcal/mol^{-1} (which is up to ~1.7 eV). He then classified the hydrogen

bonds into "strong," "moderate," and "weak" bonds based on several bond geometric parameters, such as

• The distance (H–A, in Å) between the proton (H) and the proton-acceptor group (A)
• An increased distance (Δ(D–H), in Å) between the proton (H) and the proton-donor group (D)
• The distance (D–A, in Å) between the proton-donor (D) and the proton-acceptor (A) groups
• The angle (α) of the N–H–O bond.

According to Jeffrey's criteria, all of the necessary parameters were divided into "weak" (w), "moderate" (m), and "strong" (s) class contributions. Based on this concept, we selected a set of four parameters to describe the strength of each hydrogen bond responsible for the stabilization of ammonia at the V$_2$O$_5$ surfaces according to the scheme illustrated in Table S1 of the ESM and Table 5. Based on the categorization of these four parameters, we assigned a numerical value to each bond representing its strength, with 1 representing a weak, 2 a moderately strong, and 3 a strong hydrogen bond. Moreover, for hydrogen bonds of intermediate strength, we allocated intermediate values (for example, two moderate and two strong features results in a value of 2.5). Finally, for each site, the strengths of all identified hydrogen bonds were added together and this sum was used as a site hydrogen bond strength descriptor (SHBS).

The electrostatic energy was calculated as the product of the charge on the adsorbed species (NH$_3$ or NH$_4^+$) and the electrostatic potential of the respective surface (V^{OH} or V^{bare}, respectively) at the atomic coordinates of the N atom of the adsorbed ammonia. The energy values obtained ranged from positive values (0.18 eV) for the (001) O(2) site to highly negative values for the valley adsorption site at the (001) surface (−1.54 eV). These extreme cases exemplify the effect of the electrostatic interaction on the overall energy (a decrease of E^{ads} in the case of the positive electrostatic energy for the O(2) site at the (001) net plane and an increase of E^{ads} in the case of the 4×O^e(2)O(2) site at the (001) net plane).

The results of the correlation analysis show a very high linear correlation of the adsorption energy E^{ads} with the SHBS ($R=-0.93$) and a moderate correlation with the electrostatic energy ($R=0.79$). Theoretically, both variables could be used to predict E^{ads}. However, these variables are nonorthogonal, i.e., they are linearly intercorrelated with $R=-0.82$. The collinearity indicates that multiple strong hydrogen-bonding interactions are present for sites with favorable (i.e., negative) electrostatic interactions. As a result, it is not possible to construct a QSPR model with these two variables; because of the collinearity problem, the electrostatic energy is statistically insignificant when used in one equation together with SHBS.

Therefore, it is not possible to independently estimate the influence of both variables on the adsorption energy. Because

Table 5 Parameters used in the hydrogen-bond analysis. E^{ads}: ammonia adsorption energy, D: proton donor species, $H\cdots A$: distance between the hydrogen atom and the hydrogen bond acceptor, $D\cdots A$: distance between the donor and acceptor, $\Delta(D–H)$: change in donor-hydrogen atom bond length upon hydrogen-bond formation, α: $D\cdots H\cdots A$ angle. The strength of a particular Jeffrey hydrogen bonding criterion is shown using color: *black* for strong, *gray* for moderately strong, and *white* for weak

hydrogen bonds. The number representing the hydrogen-bond strength is provided in the hydrogen-bond strength column, whereas the site hydrogen bond strength (SHBS) provides the sum of the strengths of all hydrogen-bond interactions in a particular binding site. *Elect. energy*: electrostatic energy calculated at the atomic coordinates of the N atom of the adsorbed ammonia over the respective surface

surface	Adsorption center	E^{ads} [eV]	D	$H\cdots A$ [Å]	$D\cdots A$ [Å]	$\Delta(D-H)$ [Å]	α [°]	H-bond strength	Site H-bond strength (SHBS)	Elect. energy [eV]
010	O(1)	-1.31	NH₄	1.55	2.51	0.02	170	2.75	4.75	-0.51
	O(1)			1.70	2.72	0.05	155	2		
	O(2)	-0.98	NH₄	1.48	2.60	0.09	175	2.75	2.75	-0.57
	O(3)	-1.07	NH₄	1.55	2.63	0.07	165	2.25	4	-0.52
	O(2)			2.03	2.84	0.01	133	1.75		
100	O(1)	-0.86	NH₄	1.38	2.54	0.14	179	2.75	2.75	-0.69
	O(2)	-0.70	NH₄	1.55	2.67	0.085	175	2.5	4	-0.72
	O(2)			1.9	2.95	0.025	178	2		
001	O(2)	-0.49	OH	1.83	2.80	0.04	159	2	2	0.18
	Oᵉ(2)	-1.97	NH₄	1.63	2.70	0.04	173	2.5	8.5	-1.54
	Oᵉ(2)			1.66	2.72	0.04	174	2.5		
	Oᵉ(2)			2.91	3.72	0	135	1		
	O(1)			2.94	3.64	0	126	1		
	O(1)			2.98	3.93	0	154	1.25		

more of the variance of the E^{ads} value can be explained by SHBS ($R^2=0.87$), this descriptor can be used to approximate the energy using the following simple QSPR model:

$$E^{ads} = -0.21(\pm 0.037)\text{SHBS} - 0.20(\pm 0.17)$$
$$n = 7 \quad R^2 = 0.8609, \text{corr.} \ R^2 = 0.8331, \quad F = 30.996, \quad p = 0.00258.$$

The same model is obtained for DFT+D2 corrected adsorption energies ($R^2=0.87$, corr. $R^2=0.84404$, $F=33.472$, $p<0.00217$), where London dispersion forces are accounted for with a more negative constant (−0.44 instead of −0.2).

$$E^{ads(\text{DFT}+\text{D2})} = -0.21(\pm 0.036)\text{SHBS} - 0.44(\pm 0.17.)$$

This result indicates that introducing DFT+D2 corrections on average does not cause any significant change to the observed trend.

The QSPR model demonstrates that higher hydrogen-bond strengths at the particular site result in lower adsorption energies. The quality of the model's predictions is graphically presented on a scatter plot (see Fig. 7).

The apparent success of the applied hydrogen-bond strength index in predicting the adsorption energy clearly indicates two points: (i) the importance of these interactions in the

stabilization of ammonia over V_2O_5 surfaces and (ii) the additivity of the hydrogen bonds at the particular adsorption site. However, as was demonstrated by statistical analysis, it is also important to take into account the fact that hydrogen bonds and surface electrostatic interactions are not separable,
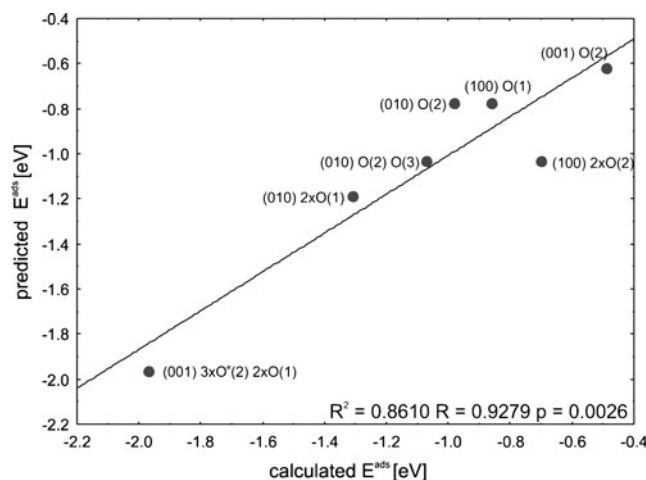

Fig. 7 Correlation scatter plot showing the predicted and DFT-calculated values for the ammonia adsorption energy ($n=7$, $R^2=0.8609$, corr. $R^2=0.8331$, $F=30.996$, $p=0.00258$)

independent phenomena. If a nondirectional positive electrostatic interaction exists, it allows for the formation of stronger, shorter hydrogen bonds. In contrast, when a repulsive interaction with the surface adsorbate occurs, the hydrogen bonds should be elongated, weakening the overall interaction. This relationship explains the high negative linear correlation that was observed between SHBS and the electrostatic energy at the adsorption site.

Conclusions

Based on the theoretical results, we can conclude that not only the saturated (010) but also the two unsaturated (001) and (100) surfaces are able to stabilize ammonia by adsorbing it at Brønsted acid sites, i.e., at OH surface groups. In all cases, the hydrogen bonds play a major role in this process.

Hydrogen bonds are formed via two different adsorption mechanisms. In the dominant scheme, a surface proton from the OH group is abstracted during ammonia adsorption and shifted toward the ammonia to become an NH_4^+ cation that serves as a "proton-donor" group in the newly created hydrogen bond. In the second scheme, no proton transfer is observed during the NH_3 adsorption; consequently, a surface hydroxyl species serves as the proton-donor group.

The local electrostatic interaction and the change in this interaction following proton transfer from the surface to the ammonia (when approaching the Brønsted site) appear to determine the adsorption mechanism. The electrostatic interactions between the catalyst surface and the adsorbing species also contribute to the overall stabilization, although it was not possible to evaluate the influence of these interactions on the adsorption energy independently of the input introduced by hydrogen bonding. The magnitude of this contribution strongly depends on the surface and is the largest for the negatively charged "valley" region of the (001) net plane (-1.97 eV). The adsorption energies of ammonia correlate very well with the hydrogen-bond strengths of the site. The strength of the hydrogen-bond stabilization can be derived only from geometrical features such as angles and atomic distances.

Finally, the results of our calculations fully confirm the previous predictions that the active sites for ammonia activation in the SCR mechanism are localized not only at saturated (010) sites but also at the unsaturated (001) and (100) V_2O_5 surfaces.

References

1. Bosch H, Janssen F (1988) Formation and control of nitrogen oxides. Catal Today 2(4):369–379
2. Topsoe N-Y (1991) Characterization of the nature of surface sites on vanadia–titania catalysts by FTIR. J Catal 128(2):499–511
3. Cai Y, Ozkan US (1991) Vanadia/titania catalysts in selective catalytic reduction of nitric oxide with ammonia. Appl Catal 78(2):241–255
4. Topsoe NY, Topsoe H, Dumesic JA (1995) Vanadia/titania catalysts for selective catalytic reduction (SCR) of nitric oxide by ammonia: I. Combined temperature-programmed in-situ FTIR and on-line mass-spectroscopy studies. J Catal 151(1):226–240
5. Dumesic JA, Topsøe NY, Topsøe H, Chen Y, Slabiak T (1996) Kinetics of selective catalytic reduction of nitric oxide by ammonia over vanadia/titania. J Catal 163(2):409–417
6. Lietti L, Forzatti P, Bregani F (1996) Steady-state and transient reactivity study of TiO_2-supported V_2O_5–WO_3 De-NOx catalysts: relevance of the vanadium−tungsten interaction on the catalytic activity. Ind Eng Chem Res 35(11):3884–3892
7. Lietti L, Alemany JL, Forzatti P, Busca G, Ramis G, Giamello E, Bregani F (1996) Reactivity of V_2O_5–WO_3/TiO_2 catalysts in the selective catalytic reduction of nitric oxide by ammonia. Catal Today 29(1–4):143–148
8. Duffy BL, Curry-Hyde HE, Cant NW, Nelson PF (1994) Isotopic labeling studies of the effects of temperature, water, and vanadia loading on the selective catalytic reduction of NO with NH_3 over vanadia–titania catalysts. J Phys Chem 98(29):7153–7161
9. Ramis G, Yi L, Busca G, Turco M, Kotur E, Willey RJ (1995) Adsorption, activation, and oxidation of ammonia over SCR catalysts. J Catal 157(2):523–535
10. Hu S, Apple TM (1996) ^{15}N NMR study of the adsorption of NO and NH_3 on titania-supported vanadia catalysts. J Catal 158(1):199–204
11. Pinaeva LG, Suknev AP, Budneva AA, Paukshtis EA, Bal'zhinimaev BS (1996) On the role of oxygen in the reaction of NO reduction by NH_3 over monolayer V_2O_5–TiO_2 catalyst. J Mol Catal A Chem 112(1):115–124
12. Tronconi E, Lietti L, Forzatti P, Malloggi S (1996) Experimental and theoretical investigation of the dynamics of the SCR–DeNOx reaction. Chem Eng Sci 51(11):2965–2970
13. Qi G, Yang RT (2005) Low-temperature SCR of NO with NH_3 over noble metal promoted Fe-ZSM-5 catalysts. Catal Lett 100(3):243–246
14. Pârvulescu VI, Grange P, Delmon B (1998) Catalytic removal of NO. Catal Today 46(4):233–316
15. Busca G, Lietti L, Ramis G, Berti F (1998) Chemical and mechanistic aspects of the selective catalytic reduction of NOx by ammonia over oxide catalysts: a review. Appl Catal B 18(1–2):1–36
16. Bond GC, Forzatti P, Védrine JC (2000) General introduction: origins and objectives of the study. Catal Today 56(4):329–332
17. Coudurier G, Védrine JC (2000) EUROCAT oxide: an European V_2O_5–WO_3/TiO_2 SCR standard catalyst study: characterisation by electron microscopies (SEM, HRTEM, EDX) and by atomic force microscopy. Catal Today 56(4):415–430
18. Calatayud M, Mguig B, Minot C (2004) Modeling catalytic reduction of NO by ammonia over V_2O_5. Surf Sci Rep 55(6–8):169–236
19. Tronconi E, Nova I, Ciardelli C, Chatterjee D, Weibel M (2007) Redox features in the catalytic mechanism of the "standard" and "fast" NH_3-SCR of NOx over a V-based catalyst investigated by dynamic methods. J Catal 245(1):1–10

20. Goo JH, Irfan MF, Kim SD, Hong SC (2007) Effects of NO_2 and SO_2 on selective catalytic reduction of nitrogen oxides by ammonia. Chemosphere 67(4):718–723

21. Koebel M, Madia G, Elsener M (2002) Selective catalytic reduction of NO and NO_2 at low temperatures. Catal Today 73(3–4):239–247

22. Koebel M, Madia G, Raimondi F, Wokaun A (2002) Enhanced reoxidation of vanadia by NO_2 in the fast SCR reaction. J Catal 209(1):159–165

23. Madia G, Koebel M, Elsener M, Wokaun A (2002) Side reactions in the selective catalytic reduction of NOx with various NO_2 fractions. Ind Eng Chem Res 41(16):4008–4015

24. Inomata M, Miyamoto A, Murakami Y (1980) Mechanism of the reaction of NO and NH_3 on vanadium oxide catalyst in the presence of oxygen under the dilute gas condition. J Catal 62(1):140–148

25. Inomata M, Miyamoto A, Ui T, Kobayashi K, Murakami Y (1982) Activities of vanadium pentoxide/titanium dioxide and vanadium pentoxide/aluminum oxide catalysts for the reaction of nitric oxide and ammonia in the presence of oxygen. Ind Eng Chem Prod Res Dev 21(3):424–428

26. Miyamoto A, Yamazaki Y, Hattori T, Inomata M, Murakami Y (1982) Study on the pulse reaction technique: VI. Kinetics of the reaction of NO with NH_3 on a V_2O_5 catalyst. J Catal 74(1):144–155

27. Miyamoto A, Kobayashi K, Inomata M, Murakami Y (1982) Nitrogen-15 tracer investigation of the mechanism of the reaction of nitric oxide with ammonia on vanadium oxide catalysts. J Phys Chem 86(15):2945–2950

28. Lietti L, Svachula J, Forzatti P, Busca G, Ramis G, Bregani P (1993) Surface and catalytic properties of vanadia–titania and tungsta–titania systems in the selective catalytic reduction of nitrogen oxides. Catal Today 17(1–2):131–139

29. Lietti L, Ramis G, Berti F, Toledo G, Robba D, Busca G, Forzatti P (1998) Chemical, structural and mechanistic aspects on NOx SCR over commercial and model oxide catalysts. Catal Today 42(1–2):101–116

30. Lietti L, Nova I, Tronconi E, Forzatti P (1998) Transient kinetic study of the SCR-DeNOx reaction. Catal Today 45(1–4):85–92

31. Casagrande L, Lietti L, Nova I, Forzatti P, Baiker A (1999) SCR of NO by NH_3 over TiO_2-supported V_2O_5–MoO_3 catalysts: reactivity and redox behavior. Appl Catal B 22(1):63–77

32. Odriozola JA, Heinemann H, Somorjai GA, de la Banda JFG, Pereira P (1989) AES and TDS study of the adsorption of NH_3 and NO on V_2O_5 and TiO_2 surfaces: mechanistic implications. J Catal 119(1):71–82

33. Odriozola JA, Soria J, Somorjai GA, Heinemann H, Garcia de la Banda JF, Lopez Granados M, Conesa JC (1991) Adsorption of nitric oxide and ammonia on vanadia–titania catalysts: ESR and XPS studies of adsorption. J Phys Chem 95(1):240–246

34. Centeno MA, Carrizosa I, Odriozola JA (1998) In situ DRIFTS study of the SCR reaction of NO with NH_3 in the presence of O_2 over lanthanide-doped V_2O_5/Al_2O_3 catalysts. Appl Catal B 19(1):67–73

35. Janssen FJJG, Van den Kerkhof FMG, Bosch H, Ross JRH (1987) Mechanism of the reaction of nitric oxide, ammonia, and oxygen over vanadia catalysts. I. The role of oxygen studied by way of isotopic transients under dilute conditions. J Phys Chem 91(23):5921–5927

36. Janssen FJJG, Van den Kerkhof FMG, Bosch H, Ross JRH (1987) Mechanism of the reaction of nitric oxide, ammonia, and oxygen over vanadia catalysts. 2. Isotopic transient studies with oxygen-18 and nitrogen-15. J Phys Chem 91(27):6633–6638

37. Ramis G, Yi L, Busca G (1996) Ammonia activation over catalysts for the selective catalytic reduction of NOx and the selective catalytic oxidation of NH_3. An FT-IR study. Catal Today 28(4):373–380

38. Schneider H, Tschudin S, Schneider M, Wokaun A, Baiker A (1994) In situ diffuse reflectance FTIR study of the selective catalytic reduction of NO by NH_3 over vanadia–titania aerogels. J Catal 147(1):5–14

39. Ozkan US, Cai Y, Kumthekar MW (1993) Effect of crystal morphology in selective catalytic reduction of nitric oxide over V_2O_5 catalysts. Appl Catal A 96(2):365–381

40. Ozkan US, Cai YP, Kumthekar MW, Zhang LP (1993) Role of ammonia oxidation in selective catalytic reduction of nitric oxide over vanadia catalysts. J Catal 142(1):182–197

41. Ozkan US, Cai YP, Kumthekar MW (1994) Investigation of the reaction pathways in selective catalytic reduction of NO with NH_3 over V_2O_5 catalysts: isotopic labeling studies using $^{18}O_2$, $^{15}NH_3$, ^{15}NO, and $^{15}N^{18}O$. J Catal 149(2):390–403

42. Gasior M, Haber J, Machej T, Czeppe T (1988) Mechanism of the reaction NO+NH_3 on V_2O_5 catalysts. J Mol Catal 43(3):359–369

43. Takagi-Kawai M, Kawai T, Soma M, Onishi T, Tamaru K (1979) Reply to Akira Miyamoto et al. J Catal 57(3):528–528

44. Takagi M, Kawai T, Soma M, Onishi T, Tamaru K (1977) The mechanism of the reaction between NOx and NH_3 on V_2O_5 in the presence of oxygen. J Catal 50(3):441–446

45. Takagi M, Kawai T, Soma M, Onishi T, Tamaru K (1976) Mechanism of catalytic reaction between nitric oxide and ammonia on vanadium pentoxide in the presence of oxygen. J Phys Chem 80(4):430–431

46. Went GT, Leu L-J, Rosin RR, Bell AT (1992) The effects of structure on the catalytic activity and selectivity of V_2O_5/TiO_2 for the reduction of NO by NH_3. J Catal 134(2):492–505

47. Topsoe NY, Dumesic JA, Topsoe H (1995) Vanadia–titania catalysts for selective catalytic reduction of nitric-oxide by ammonia: I.I. Studies of active sites and formulation of catalytic cycles. J Catal 151(1):241–252

48. Ramis G, Busca G, Bregani F, Forzatti P (1990) Fourier transform-infrared study of the adsorption and coadsorption of nitric oxide, nitrogen dioxide and ammonia on vanadia–titania and mechanism of selective catalytic reduction. Appl Catal 64:259–278

49. Yuan R-M, Fu G, Xu X, Wan H-L (2011) Bronsted-NH_4^+ mechanism versus nitrite mechanism: new insight in the selective catalytic reduction of NO by NH_3. Phys Chem Chem Phys 13(2):453–460

50. Sun C, Dong L, Yu W, Liu L, Li H, Gao F, Dong L, Chen Y (2011) Promotion effect of tungsten oxide on SCR of NO with NH_3 for the V_2O_5–WO_3/$Ti_{0.5}Sn_{0.5}O_2$ catalyst: experiments combined with DFT calculations. J Mol Catal A Chem 346(1–2):29–38

51. Andersson A (1982) An oxidized surface state model of vanadium oxides and its application to catalysis. J Solid State Chem 42(3):263–275

52. Anstrom M, Topsøe N-Y, Dumesic JA (2003) Density functional theory studies of mechanistic aspects of the SCR reaction on vanadium oxide catalysts. J Catal 213(2):115–125

53. Anstrom M, Dumesic JA, Topsøe N-Y (2002) Theoretical insight into the nature of ammonia adsorption on vanadia-based catalysts for SCR reaction. Catal Lett 78(1):281–289

54. Kobayashi Y, Tajima N, Nakano H, Hirao K (2004) Selective catalytic reduction of nitric oxide by ammonia: the activation mechanism. J Phys Chem B 108(33):12264–12266

55. Kachurovskaya NA, Mikheeva EP, Zhidomirov GM (2002) Cluster molecular modeling of strong interaction for VOx/TiO_2 supported catalyst. J Mol Catal A Chem 178(1–2):191–198

56. Soyer S, Uzun A, Senkan S, Onal I (2006) A quantum chemical study of nitric oxide reduction by ammonia (SCR reaction) on V_2O_5 catalyst surface. Catal Today 118(3–4):268–278

57. Gilardoni F, Weber J, Baiker A (1997) Density functional investigation of the mechanism of the selective catalytic reduction of NO by NH_3 over vanadium oxide model clusters. Int J Quantum Chem 61(4):683–688

58. Gilardoni F, Weber J, Baiker A (1997) Mechanism of the vanadium oxide-catalyzed selective reduction of NO by NH_3. A quantum chemical modeling. J Phys Chem A 101(34):6069–6076

59. Yin X, Han H, Gunji I, Endou A, Cheettu Ammal SS, Kubo M, Miyamoto A (1999) NH$_3$ adsorption on the Brönsted and Lewis acid sites of V$_2$O$_5$(010): a periodic density functional study. J Phys Chem B 103(22):4701–4706

60. Yin X, Han H, Miyamoto A (2000) Active site and mechanism of the selective catalytic reduction of NO by NH$_3$ over V$_2$O$_5$: a periodic first-principles study. Phys Chem Chem Phys 2(18):4243–4248

61. Kobayashi Y, Tajima N, Hirao K (2000) A theoretical study on the reaction mechanism of the gas-phase decomposition of NO by NH$_3^+$ and NH$_4^+$. J Phys Chem A 104(29):6855–6860

62. Goclon J, Grybos R, Witko M, Hafner J (2009) Relative stability of low-index V$_2$O$_5$ surfaces: a density functional investigation. J Phys Condens Matter 21(9):095008

63. Bachmann HG, Ahmed FR, Barnes WH (1981) Z Kristallogr Kristallgeom Kristallphys Kristallchem 115:110

64. Wyckoff RWG (1965) Crystal structures. Interscience, New York

65. Hejduk P, Witko M, Hermann K (2009) Electronic structure of unsaturated V$_2$O$_5$(001) and (100) surfaces: ab initio density functional theory studies. Top Catal 52(8):1105–1115

66. Witko M, Tokarz R, Haber J (1997) Vanadium pentoxide. 2. Quantum chemical modeling. Appl Catl A Gen 157(1–2):23–44

67. Witko M, Tokarz R, Haber J (1991) The role of atoms which terminate clusters—quantum chemical study. J Mol Catal 66(3):357–366

68. Yin X, Han H, Gunji I, Endou A, Cheettu Ammal SS, Kubo M, Miyamoto A (1999) NH$_3$ adsorption on the Brönsted and Lewis acid sites of V$_2$O$_5$(010): a periodic density functional study. J Phys Chem B 103(22):4701–4706

69. Hejduk P, Szaleniec M, Witko M (2010) Molecular and dissociative adsorption of water at low-index V$_2$O$_5$ surfaces: DFT studies using cluster surface models. J Mol Catal A Chem 325(1–2):98–104

70. Gao X, Du XS, Jiang Y, Zhang Y, Luo ZY, Cen KF (2010) A DFT study on the behavior of NO$_2$ in the selective catalytic reduction of nitric oxides with ammonia on a V$_2$O$_5$ catalyst surface. J Mol Catal A Chem 317(1–2):46–53

71. Hermann K, Pettersson LGM StoBe (2008) A modified version of DFT-LCGTO program package deMon with extensions. http://www.fhi-berlin.mpg.de/~hermann/StoBe/index.html.

72. Perdew JP, Burke K, Ernzerhof M (1996) Generalized gradient approximation made simple. Phys Rev Lett 77(18):3865

73. Hammer B, Hansen LB, Norskov JK (1999) Improved adsorption energetics within density-functional theory using revised Perdew–Burke–Ernzerhof functionals. Phys Rev B 59(11):7413

74. Labanowski JK, Anzelm JW (eds) (1991) Density functional methods in chemistry. Springer, New York

75. Godbout N, Salahub DR, Andzelm J, Wimmer E (1992) Optimization of Gaussian-type basis sets for local spin density functional calculations. Part I. Boron through neon, optimization technique and validation. Can J Chem 70(2):560–571

76. Rutkowska-Zbik D, Witko M, Stochel G (2008) Ligand binding properties of cobalamins. Theor Chem Acc 120(4):411–419

77. Rutkowska-Zbik D, Witko M (2007) From activation of dioxygen to formation of high-valent oxo species: ab initio DFT studies. J Mol Catal A Chem 275(1–2):113–120

78. Rutkowska-Zbik D, Tokarz-Sobieraj R, Witko M (2007) Quantum chemical description of oxygen activation process on Co, Mn, and Mo porphyrins. J Chem Theory Comp 3(3):914–920

79. Rutkowska-Zbik D, Witko M, Stochel G (2007) Theoretical DFT studies on interactions of small biologically active molecules with isolated heme group. J Comput Chem 28:825–831

80. Rutkowska-Zbik D, Jaworska M, Witko M (2004) Application of the DFT theory to study cobalamin complexes. Struct Chem 15(5):431–435

81. Tunega D, Bucko T, Zaoui A (2012) Assessment of ten DFT methods in predicting structures of sheet silicates: importance of dispersion corrections. J Chem Phys 137(11):114105

82. Hermann K, Witko M, Druzinic R, Tokarz R (2000) Hydrogen assisted oxygen desorption from the V$_2$O$_5$(010) surface. Top Catal 11–12(1):67–75

83. Goclon J, Grybos R, Witko M, Hafner J (2009) Oxygen vacancy formation on clean and hydroxylated low-index V$_2$O$_5$ surfaces: a density functional investigation. Phys Rev B 79:07439

84. Mulliken RS (1955) Electronic population analysis on LCAO–MO molecular wave functions. I. J Chem Phys 23(10):1833–1840

85. Mayer I (1987) Bond orders and valences: role of d-orbitals for hypervalent sulphur. J Mol Struct (THEOCHEM) 149(1–2):81–89

86. Mayer I (1983) Charge, bond order and valence in the AB initio SCF theory. Chem Phys Lett 97(3):270–274

87. Grimme S (2006) Semiempirical GGA-type density functional constructed with a long-range dispersion correction. J Comput Chem 27(15):1787–1799

88. Grimme S, Antony J, Ehrlich S, Krieg H (2010) A consistent and accurate ab initio parametrization of density functional dispersion correction (DFT-D) for the 94 elements H–Pu. J Chem Phys 132(15):154104

89. University of Karlsruhe andForschungszentrum Karlsruhe GmbH (2011) TURBOMOLE v.6.3. http://www.turbomole.com.

90. Dirac PAM (1929) Quantum mechanics of many-electron systems. Proc R Soc Lond A 123(792):714–733

91. Perdew JP, Burke K, Ernzerhof M (1997) Generalized gradient approximation made simple [Phys. Rev. Lett. 77, 3865 (1996)]. Phys Rev Lett 78(7):1396–1396

92. Perdew JP, Wang Y (1992) Accurate and simple analytic representation of the electron-gas correlation energy. Phys Rev B 45(23):13244–13249

93. Slater JC (1951) A simplification of the Hartree–Fock method. Phys Rev 81(3):385–390

94. Schäfer A, Huber C, Ahlrichs R (1994) Fully optimized contracted gaussian basis sets of triple zeta valence quality for atoms Li to Kr. J Chem Phys 100(8):5829–5835

95. Eichkorn K, Treutler O, Öhm H, Häser M, Ahlrichs R (1995) Auxiliary basis sets to approximate Coulomb potentials. Chem Phys Lett 240:283–289

96. Eichkorn K, Weigend F, Treutler O, Ahlrichs R (1997) Auxiliary basis sets for main row atoms and transition metals and their use to approximate Coulomb potentials. Theor Chem Acc 97:119–124

97. Goclon J et al (2009) Relative stability of low-index V$_2$O$_5$ surfaces: a density functional investigation. J Phys Condens Matter 21(9):095008

98. Calatayud M, Tielens F, De Proft F (2008) Reactivity of gas-phase, crystal and supported V$_2$O$_5$ systems studied using density functional theory based reactivity indices. Chem Phys Lett 456(1–3):59–63

99. Tielens F, Geerlings P (2001) Henry constants predicted using multipole expansion for the interaction energies. Int J Quantum Chem 84(1):58–69

100. Jeffrey GA (1997) An introduction to hydrogen bonding. Oxford University Press, Oxford

101. Steiner T (2002) The hydrogen bond in the solid state. Angew Chem Int Ed 41(1):48–76